CPW ultra-wideband circuits for wireless communications

Mourad Nedil[1], Azzeddine Djaiz[1], Mohamed Adnane Habib[1]
and Tayeb Ahmed Denidni[2]

[1]: UQAT-LRCS, University of Quebec in Abbitibi-Témiscaminque
Canada
[2]:INRS-EMT, University of Quebec
Canada

1. Introduction

Wireless communications represent one of the highest growing markets, especially on the development of mobile communications and wireless local area networks (WLANs), where high capacity transmission systems are required. These concern new wideband RF wireless components such as antennas, filters and so on.

Recently Ultra-Wideband (UWB) radio technology has been getting more popular for high-speed wireless connectivity applications, since the Federal Communications Commission (FCC)'s decision to permit the unlicensed operation band from 3.1 to 10.6 GHz in 2002 (Stutzman et al., 1998). The UWB radio system is very promising, since transmission data rates greater than those of the other wireless LAN systems can be obtainable with less power dissipation. In this area, various studies are under progress, especially in UWB filters, which is one of the key passive components in the design of microwave circuits for UWB systems. The requirements of an UWB filter are: low insertion loss over the operating band, good performances at low frequency and outside the operating band to meet FCC's limits. Moreover, it is necessary to have a good group delay performance, which is strongly important to impulse-radio UWB systems.

The conventional RF circuits design procedures are adequate only for relatively narrowband, but they are not suitable for wideband application. In addition, the most major challenge is to design an ultra-wideband RF circuit with about 110 % percent fractional-bandwidth requirement, which makes some widely used techniques for UWB designs inefficient.

In this chapter, some UWB RF circuits will be presented and detailed. The chapter is organized as follows. After this introduction, the UWB transition and filters will be described in section II and III. In section IV, an analysis and design of a wideband directional coupler will be described. Section V, will present the UWB technique for an antenna. In the section VI, the UWB RF system will be presented. Finally, the last section presents the conclusion.

2. Ultra-wideband Transitions

Planar transmission lines such as microstrip and coplanar waveguide (CPW) have been applied in various microwave and millimeter-wave circuits. In some multilayered structures, these transmission lines coexist and are even combined to develop new circuit components (Nerguezian et al., 2005). For instance, multilayer microwave integrated circuits require more flexibility to use both microstrip and CPW circuit technologies. To ensure the compatibility between these technologies, low-loss, wideband, and compact transitions between microstrip and CPW lines are necessary.

2.1 Microstrip to CB-CPW transition

There are two main techniques for the transition between a microstrip and CPW. One is by electrical contact, and the other electromagnetic coupling (Tanaka et al., 1988; Theodorou et al., 1995). One type uses vias to connect the top layer CPW ground planes with the lower microstrip ground plane and the other does not. The transitions with via holes are compact and broadband, but the vias cause parasitic inductance and are difficult to fabricate. Existing via-less transitions are narrow band and large. Transitions by electromagnetic coupling require no wire bonds or via holes, but most of them suffer from narrow bandwidth and larger size.
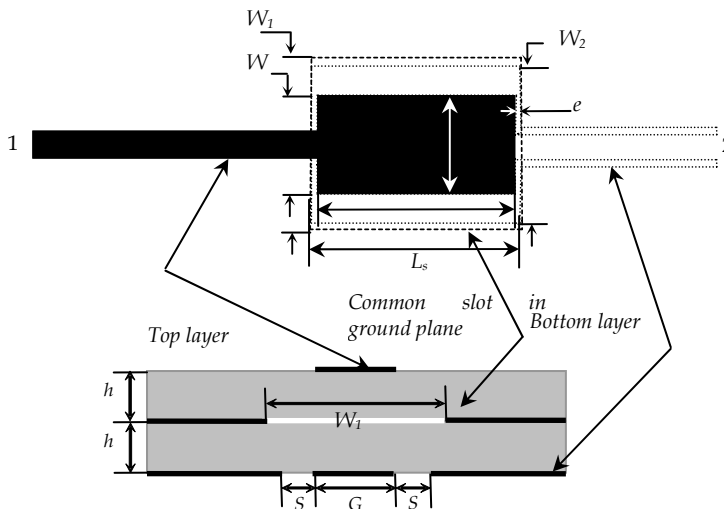

Fig. 1. Layout of the microstrip-to-CB-CPW transition.

Various approaches for transitions between microstrip and CPW lines on separate layers have been introduced such as electromagnetic coupling (Chen et al., 1996; Tran et al., 1993). In practice, additional conducting planes are often present below the substrate in order to electromagnetically separate the circuit from its environment (Tran et al., 1993). Vialess CBCPW-to-MSL transitions using electromagnetic (EM) coupling of three-line couplers have been reported (Burke et al., 1989; Zhu et al., 1999). However, the broadside CB-CPW to microstrip transition has never been proposed.
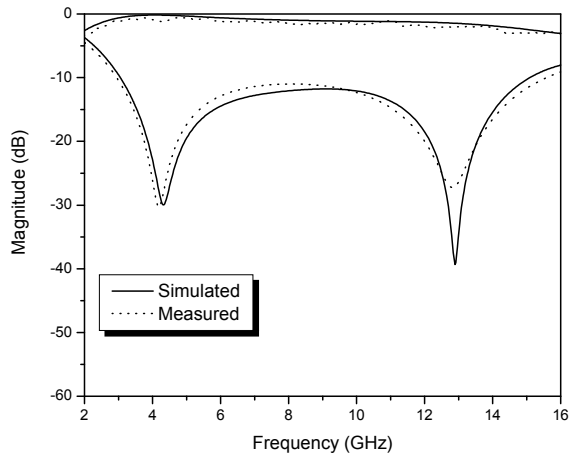
Fig. 2. Simulated and measured results of the UWB transition.

In this section, an ultra-wideband microstrip to a CB-CPW transition using the frequency-dependent behavior of surface-to-surface slot coupling is proposed.

Fig. 1 shows the geometrical layout of the proposed two-port microstrip-to-CB-CPW transition. This transition is characterized by an aperture formed on the common ground plane of the two-layered structures to provide a fed-through coupling between the upper microstrip and the lower CB-CPW lines. In this structure, the upper microstrip conductor is vertically coupled with the central strip conductor of the lower CB-CPW via a slot-coupled located in the common ground plane.

To validate the proposed approach, a prototype circuit was designed, fabricated and measured. Simulation and experimental results of the transition are shown in Fig. 2. From these curves, it can be seen that a good agreement is observed and the microstrip to CB-CPW transition offers a very wide bandwidth of ~ 12 GHz.
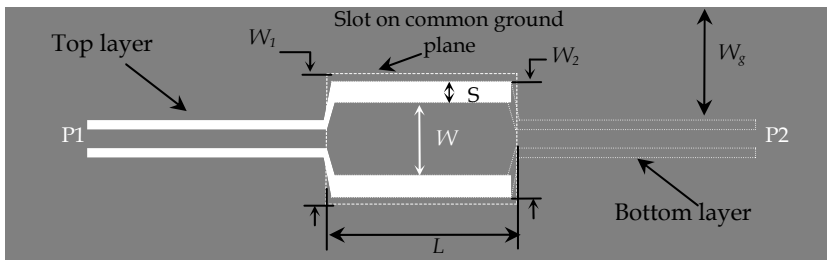
2.2 Back-to-Back CB-CPW to CB-CPW Transition

Some applications, such as multilayer microwave integrated circuits, require the flexibility to use the CPW circuits in deferent layers. Therefore, low-loss, wideband, and compact transitions between these layers are necessary to ensure good compatibility. In this area, vertical interconnections between various signal lines in different layers are often needed in a multilayer circuit environment. In this area, printed slots have been suggested to be versatile for vertical transitions. They can be implemented to couple electromagnetic energy from one side of a circuit module to another separated by a common conductor. The conductor backed coplanar waveguide (CBCPW) technology is an attractive option because it provides the benefit of added mechanical support and heat sinking ability compared to conventional CPW. Few works on CBCPW-to-CBCPW transitions have been done. However, these transitions are based only on via connections.

In this subsection, a new type of CBCPW-to-CBCPW transition based on the concept of slot coupling in the common ground plane will be presented. This transition is characterized by

an aperture etched on the common ground plane of the two stacked layer CBCPW lines to provide a fed-through coupling between the upper CBCPW line and the lower CB-CPW line. This transition can offer advantages of broad bandwidth, compact size, low fabrication cost, and high reliability.
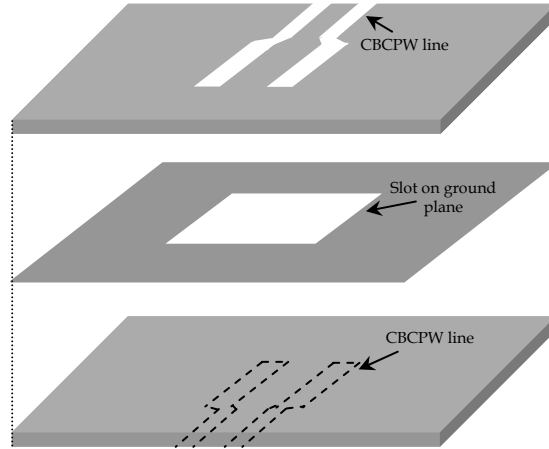
(a)

(b)

Fig. 3. Layout of the CB-CPW-to-CB-CPW transition.

Fig. 3 shows the geometrical layout of the proposed two-port CBCPW-to-CBCPW transition. This arrangement of the back-to-back CBCPW transition allows the both transmission lines to share a common ground plane. Each CBCPW line is formed by abruptly ending the slots as shown in Fig. 3. As a result, an RF current flows around the end of the slot, and therefore magnetic energy is stored behind the termination. Then, this energy is coupled via a rectangular slot located in the common ground plane from the top layer line to second line located in the bottom layer.

To verify the performances of the proposed design, a back-to-back prototype transition was fabricated, and the scattering parameters were measured. Simulation and experimental results of the transition are shown in Fig. 4. From these curves, it can be seen that the comparison between simulated and experimental data shows a good agreement, and the CBCPW-to-CBCPW transition offers a very wide bandwidth of ~ 12 GHz, which operates well over almost the entire band of 3-15 GHz.
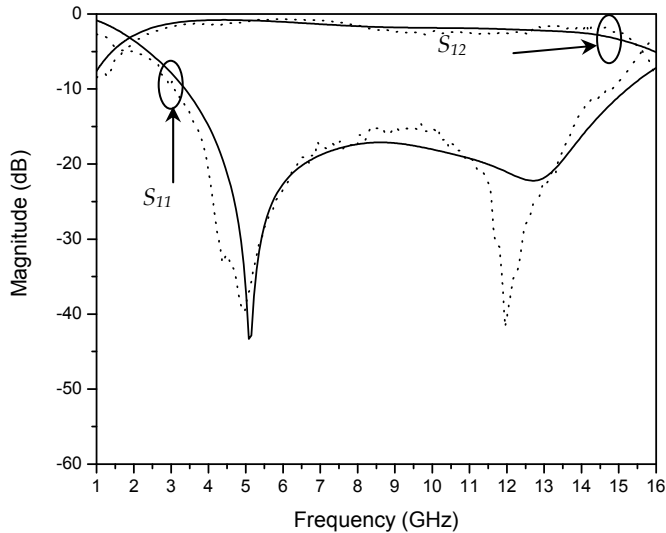

Fig. 4. Simulated and measured results of the CB-CPW transition.

3. Ultra-Wideband Filters

The conventional filter synthesis procedure is adequate only for the relatively narrowband filters, and it is not suitable for the wideband filters. In addition, the most difficult problem is to design ultra-wideband filter with about 110 % percent fractional-bandwidth requirement, which makes some widely used techniques for UWB designs inapplicable.

3.1 Ultra-Wideband Filter Design Based on CPW-to-Microstrip transition

As mentioned, the most challenging problem in the design of UWB filter is the 110 % bandwidth requirement. For this issue, an UWB filter design is introduced. Fig. 5 shows the layout of the proposed filter. The filter structure is based on the back-to-back microstrip-to-CB-CPW transition described in the previous section. The filter is composed of two CBCPW to microstrip transitions and a microstrip line section, which is used as a multiple-mode (MMR) resonator between the two transitions. At the center frequency of the concerned UWB passband, both side sections of this MMR (CBCPW to microstrip transitions) are

identical, and they are chosen as one quarter-wavelength ($\lambda_g/4$) while the middle section is set as one half-wavelength ($\lambda_g/2$).
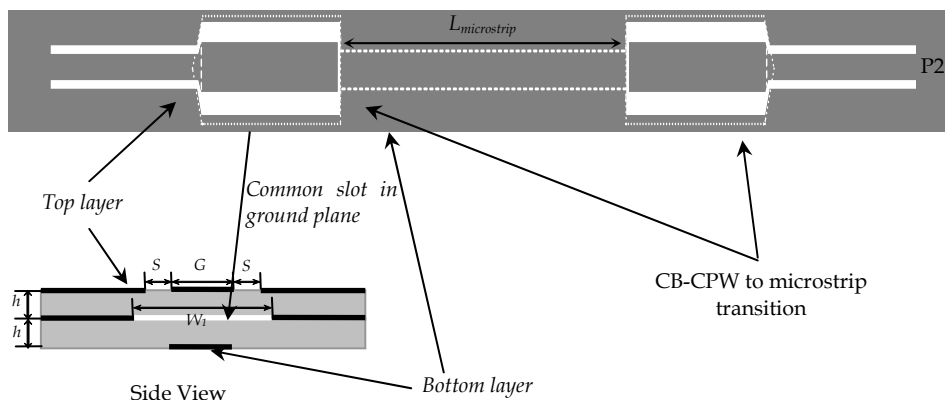

Fig. 5. Layout of the CBCPW fed UWB filter

Numerical simulations on the filter were carried out with the electromagnetic simulator ADS MOMENTUM. In these simulations, it is found that the out-of-band rejection at high frequencies can be improved by optimizing both CB-CPW and microstrip line of the transitions. To optimize the performance of the proposed filter, a parametric study was also performed and the optimal dimensions of the proposed filter are determined, in which $L_{microstrip}$ = 15.5 mm, L = 7.8 mm, L_S = 8.1 mm, W = 1.4 mm, W_1 = 3.13 mm, W_2 = 2.68 mm, G = 1.83 mm, e = 0.15mm.

Fig. 6. Photograph of the fabricated UWB filter.

The fabricated filter was measured using a network analyzer HP8720, and its photograph is shown in Fig. 6. The simulated and measured results are shown in Fig. 7. It can be seen that the measured results agree well with the simulated ones. Both the measured and the simulated results show that, the proposed filter has a small insertion loss.

Fig. 8 shows the simulated and measured results of the group delay. The group delay varies between 0.3 and 0.50 ns with a maximum variation of 0.2 ns, which leads to good linearity of the proposed UWB filter. The group delay of the proposed filter is found to be lower than that of the hybrid microstrip/CPW filter. From these results, it can be concluded that the proposed filter satisfies the requirements of a small and flat group delay over the operating band, which is strongly required for impulse radio systems to minimize the distortion in short pulse transmission system.
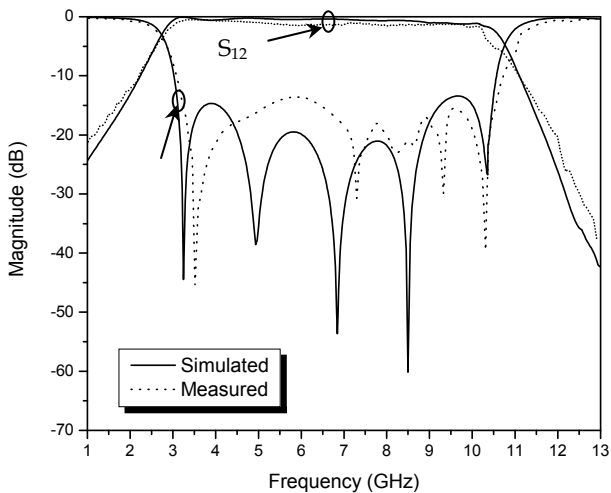
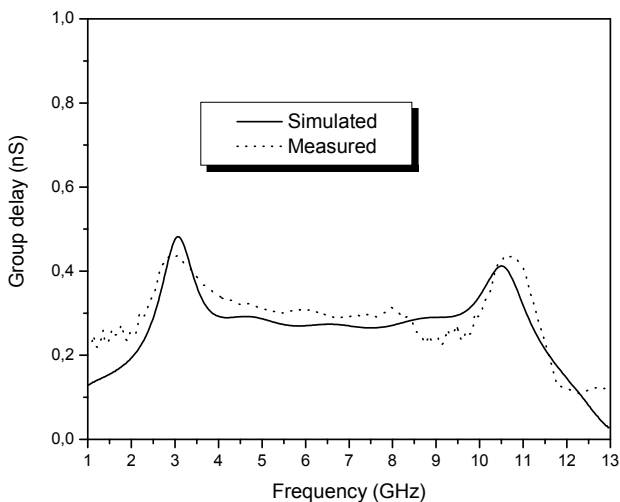Fig. 7. Simulated and measured results of the UWB filter.

Fig. 8. Simulated and measured results of the group delay of the UWB filter.

3.2 Microstrip fed Ultra-Wideband Filter
Similarly with the UWB filter introduced earlier, the second filter is composed of two microstrip–CBCPW transitions and a section of CBCPW transmission line is designed. The CBCPW feed line and the microstrip line are replaced by microstrip feed line and a section

of CBCPW, respectively to generate the multi-mode resonator (MMR). At the central frequency of the concerned UWB passband, the two side sections of this MMR are equally selected as one quarter-wavelength while the central section is set as one half-wavelength ($\lambda g_0/2$) long. As such, the second resonant frequency of this MMR can be readily allocated around 6.85GHz.

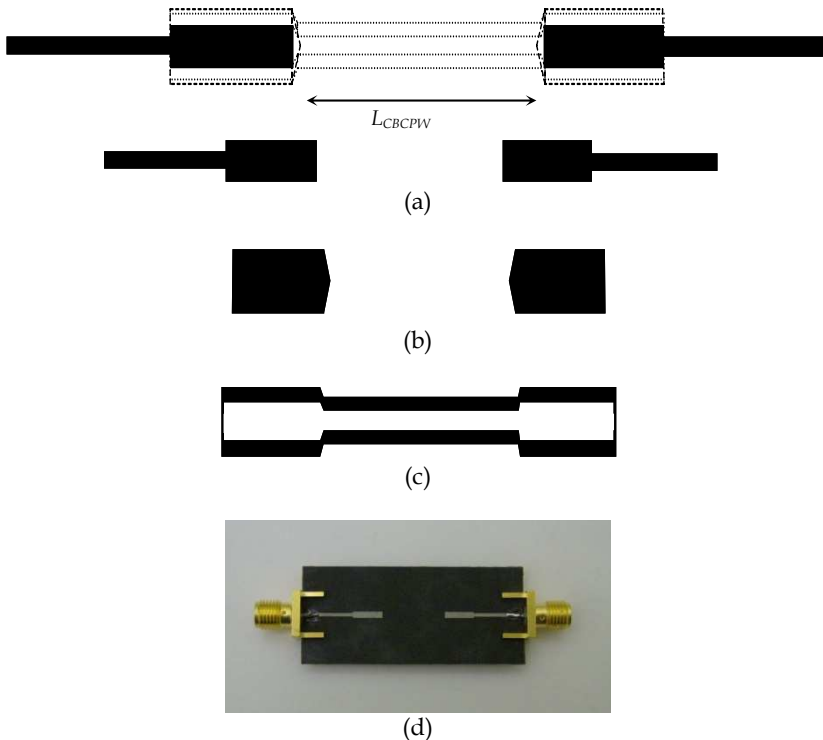L_{CBCPW}

(a)

(b)

(c)

(d)

Fig. 9. Layout of the UWB filter (a) Top layer (b) Common slot in ground plane (c) Bottom layer (d) Fabricated filter.

The fabricated filter is illustrated in Fig. 9. The simulated and measured results are shown in Fig. 10. It can be seen that the measured results agree well with the simulated ones. Both the measured and the simulated results show that, in the in-band performance, a small insertion loss. This filter presents a good performance in terms of return loss compared to the first filter design.

Fig. 11 shows the simulated and measured results of the group delay of this filter which is about 0.3 nS. From these results, it may be concluded that this filter is similar to the first UWB filter in terms of small and flat group delay.

It can be seen that for each filter, the optimum out-of-band rejection should be improved especially in low frequencies.
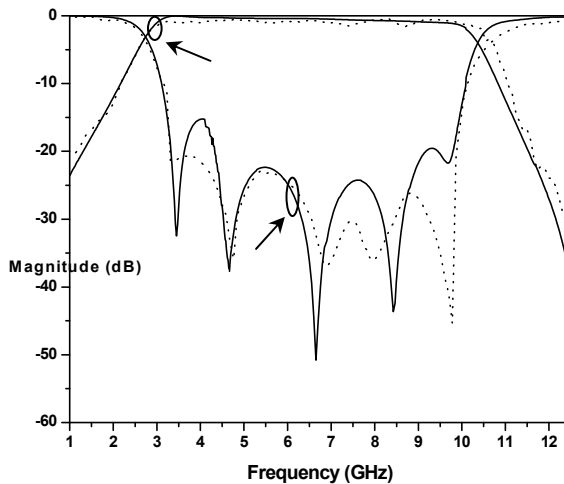
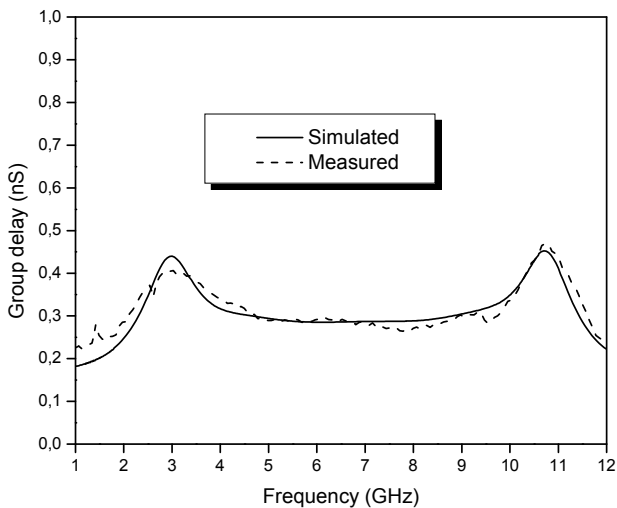Fig. 10. Simulated and measured results of the proposed UWB filter.

Fig. 11. Simulated and measured results of group delay of the UWB filter.

4. Ultra-Wideband Directional Coupler

Directional couplers are fundamental and indispensable components used in microwave integrated circuits applications. Indeed, these components are often used in microwave systems to combine or divide RF signals, and they are commonly applied in many applications, such as antenna feeds, balanced mixers, modulators and so on.

Tight-coupling directional couplers are often required in the design of various multiport circuits or beamforming networks of antenna arrays. In the practical issue, these couplers should be compact in order to be easily integrated with other components in the same circuit. For instance, the microstrip branch line couplers or hybrid ring couplers have extensively been employed in printed microstrip array feeding networks (Tudosie et al., 2006). However, these couplers have inherently narrow bandwidths.

To overcome this situation, CPW technology has been proposed to implement various couplers. Indeed, CPW technology offers several attractive features: absence of costly and inductive via holes, ease of making shunt and series connections, ease of controlling the characteristics of CPW lines by changing the slot and strip widths, and possible implementability at millimeter-waves applications. Furthermore, directional couplers with CPW structures can also provide a higher directivity. Using this technology, different configurations of CPW directional couplers have been proposed (Lim et al., 1999). Moreover, to improve directional coupler performances, the conductor-backed coplanar waveguide technology was also proposed to reduce the coupler size and to avoid air bridges used to connect ground planes of the conventional CPW technology (Lim et al., 1999). In this area, few works on CB-CPW couplers have been reported in literature [6-9]. A 3-dB CB-CPW coupled-line directional coupler has been used in tunable analog phase shifting [6]. A finite-extent backed conductor on the other side of the substrate is added to the conventional edge-coupled CPW structure has been suggested in [7] to enhance the coupling. Recently, broadside CB-CPW directional coupler has been proposed in [8]. However, this coupler has not been optimized to have the maximum of bandwidth to covers ultra-wideband applications.

In this section, a wideband multilayer directional coupler using slot-coupled technique is proposed.

Fig. 12a shows the layout of the proposed hexagonal slot-coupled directional coupler. It allows coupling two CPW lines placed in different layers through a rectangular slot etched on the common ground plane.

4.1 Quasi-Static Coupler Analysis

For the analysis of this work, it is assumed that the proposed configuration has a ground plane with infinite size and all conductors are perfect. This structure supports both fundamental modes, namely odd and even. The even and odd-mode coupler impedances, Z_{e0} and Z_{o0}, are calculated using conformal mapping techniques to determine the coupler capacitance per unit length for even and odd-modes. These modes are illustrated in Fig. 12b. These modes can be isolated by assuming an electrical wall for the odd mode and a magnetic wall for the even mode. For each mode, the structure is analyzed in a manner similar that reported in [8]. In this section, expressions for the effective dielectric constant as well as the characteristic impedance for the odd and even modes obtained using the quasi-static conformal mapping technique will be presented.
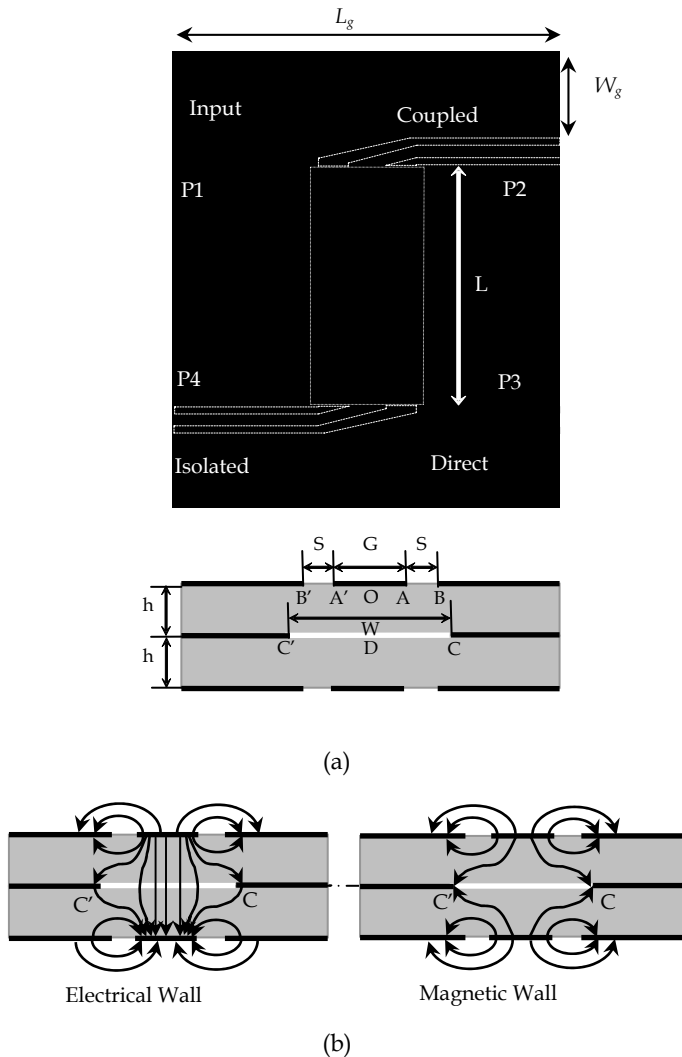
(a)

(b)

Fig. 12. Broadside directional slot-coupled coupler: (a) Layout (b) Odd and even-mode electric field distribution.

For the odd-mode excitation, an electrical wall is placed in the plane of symmetry (CC') as shown in Fig. 13. The analysis is then restricted to upper half of the structure. Then, the total odd-mode capacitance per unit length can then be considered as the sum of two components, C_{o1}, C_{o2}, representing the electrical field in the upper region (air) and middle region (dielectric), respectively.
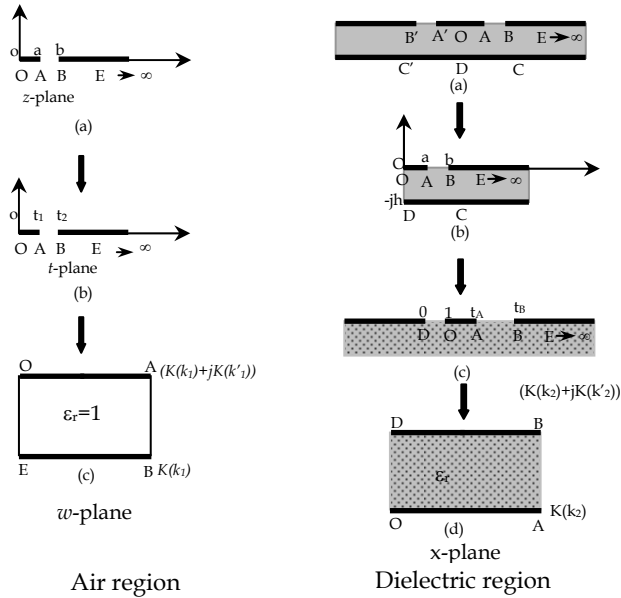
Fig. 13. Conformal mapping transformation of the odd-mode

a) Odd Mode (air)

The Schwarz-Christoffel transformation can be done from the t-plane to the w-plane (Fig. 13). The transformation equation for the configuration with only air above the interface is given by

$$t = z^2 \tag{1}$$

The Schwarz-Christoffel integral is then

$$w = \int_{t_0}^{t} \frac{dt}{\sqrt{t(t-t_1)(t-t_2)}} \tag{2}$$

The capacitance per unit length C_{01} is then obtained as

$$C_{o1} = 2\varepsilon_0 \frac{\overline{OA}}{\overline{AB}} = 2\varepsilon_0 \frac{K(k_0)}{K'(k_0)} \tag{3}$$

The argument k_0 is :

$$k_0 = \frac{a}{b} = \frac{G}{G + 2S} \tag{4}$$

where $K(k_0)$ and $K(k'_0)$ are the complete elliptical of the first kind and its complement. The accurate expression for the ratio $K(k_0)/K(k'_0)$ have been reported in [9]. These are given below:

$$\frac{K(k)}{K(k')} = \frac{\pi}{\ln\left[\dfrac{2(1+\sqrt{k'_0})}{1-\sqrt{k'_0}}\right]} \qquad \text{if } 0 \leq k \leq 0.707 \tag{5.a}$$

$$\frac{K(k)}{K(k')} = \frac{1}{\pi}\ln\left[\frac{2(1+\sqrt{k_0})}{1-\sqrt{k_0}}\right] \qquad \text{if } 0.707 \leq k \leq 1 \tag{5.b}$$

with $\quad k'_0 = \sqrt{1-k_0^{\,2}}$

These expressions are the same for the even-mode in the air case.

b) Odd Mode (dielectric)
As shown in Fig. 13, an electric wall is assumed to be present at CC' plane of the structure in the dielectric region. The configuration is first converted into the t-plane by the following expression:

$$t = \cosh^2(\frac{\pi z}{2h}) \tag{6}$$

$$C_{o2} = 2\varepsilon_r \varepsilon_0 \frac{K(k_1)}{K'(k_1)} \tag{7}$$

$$k_1 = \frac{\tanh\left(\dfrac{\pi a_1}{2h}\right)}{\tanh\left(\dfrac{\pi b_1}{2h}\right)} \tag{8}$$

with $a_1 = t_A$ and $b_1 = t_B$

The total capacitance C_{oT} is obtained as:

$$C_{oT} = C_{o2} + C_{o1} \tag{9}$$

The odd-mode permittivity $\varepsilon_{\text{oeff}}$ is defined as [9],

$$\varepsilon_{o,eff} = \frac{C_{oT}(\varepsilon_r)}{C_{oT}(\varepsilon_r)} \tag{10}$$

The odd-mode characteristic impedance is given by [9]:

$$Z_{o,0} = \frac{60\pi}{\sqrt{\varepsilon_{o,eff}}\left[\dfrac{K(k_0)}{K(k'_0)} + \dfrac{K(k_1)}{K(k'_1)}\right]}$$ (11)

c) Even Mode (dielectric)

The even-mode dielectric is assured by considering the magnetic wall in the section (CC'). The electrical field of the coupler in the even-mode show that we can replace the symmetrical half-plane structure with quarter-plane with taken electrical wall (OD) into account (see Fig. 14b).

The analysis of the even-mode is similar to the odd-mode. Fig. 14 shows the progression from the Z-plane, to an intermediate stage in the t-plane, and finally to a parallel-plate capacitor in the x-plane. The configuration in Fig. 14a is first converted into the one shown in Fig. 14b, by mapping expression (6).The asymmetrical line configuration in Fig. 14c is transformed into symmetrical line configuration, as shown in Fig. 14d [11].

$$C_{e2} = 2\varepsilon_r\varepsilon_0 \frac{K(k_4)}{K'(k_4)}$$ (12)

$$k_4 = \sqrt{\frac{2a_1(b_1+b_2)}{(a_1+b_1)(a_1+b_2)}}$$ (13)

with $a_1 = t_A = \cosh^2(\dfrac{\pi G}{4h})$, $b_1 = t_B = \cosh^2(\dfrac{\pi(S+G/2)}{2h})$ and $b_2 = -t_c = \sinh^2(\dfrac{\pi W}{4h})$

The total capacitance C_{oT} of the odd-mode case is:

$$C_{eT} = C_{o2} + C_{e1}$$ (14)

The odd-mode permittivity ε_{oeff} is defined as,

$$\varepsilon_{e,eff} = \frac{C_{eT}(\varepsilon_r)}{C_{eT}(\varepsilon_r)}$$ (15)

The odd-mode characteristic impedance is given by

$$Z_{e,0} = \frac{60\pi}{\sqrt{\varepsilon_{e,eff}}\left[\dfrac{K(k_3)}{K(k'_3)} + \dfrac{K(k_4)}{K(k'_4)}\right]}$$ (16)

The coupling coefficient *K* expressed as:

$$K = \frac{Z_{0,e} - Z_{0,o}}{Z_{0,e} + Z_{0,o}} \tag{17}$$
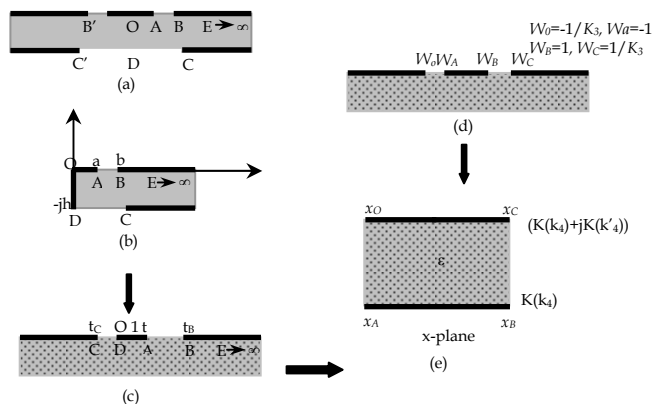

Fig. 14. Conformal mapping transformation of the even-mode in the dielectric region.

4.2 Results and Discussion

Numerical results of odd-mode characteristic impedances of the CPW multilayer slot coupled-coupler are plotted in Fig. 15, versus the normalized gap width *S*/h and normalized strip width *G*/h. It is seen that, for a fixed substrate thickness, as the gap width (*S*) the odd-mode characteristic impedance is increased, whereas those while the strip conductor width (*G*) increases, the odd-mode characteristic impedance $Z_{0,o}$ decrease. In fact, the odd-mode parameters change slowly as the gap width is increased up to a certain limit.

The variation of the even-mode characteristic impedance can be expressed as a function of the normalized gap width *S*/h, the normalized slot-coupled width *W*/h and *W*/G are shown in Fig. 16. As can be seen for a fixed strip conductor and thickness *(G, h)*, $Z_{e,0}$ while increases the slot-coupled width (*W*) increases.
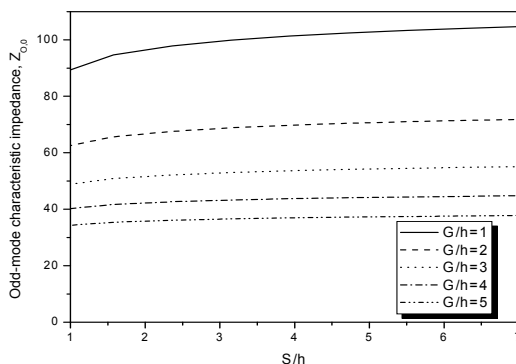

Fig. 15. Odd-mode characteristic impedance

(a)   (b)
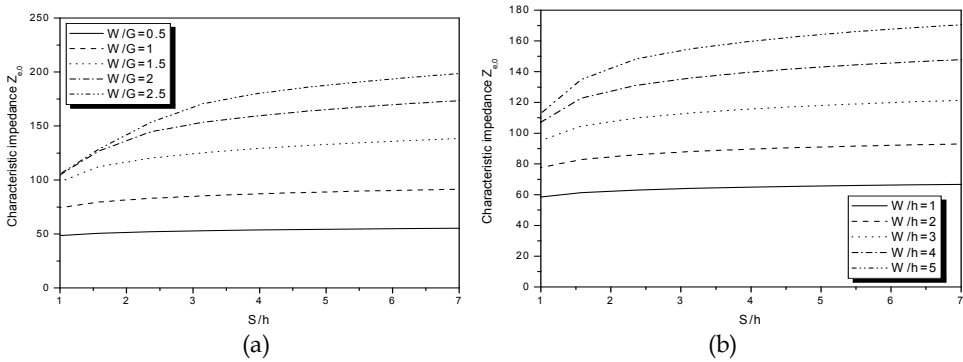
Fig. 16. Even-mode characteristic impedance as a function of (a) *W/G* (b) *W/h*
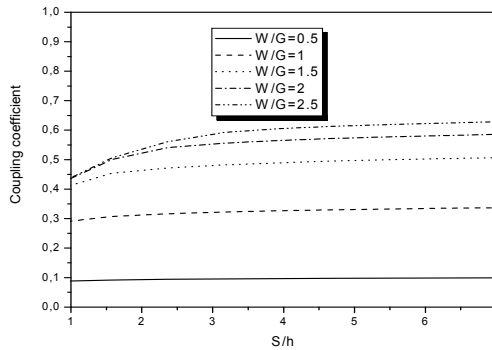

Fig. 17. Coupling coefficient

In addition, it is shown that the slot-coupled width *W* affect considerably the characteristic impedance $Z_{0,e}$ (see Fig. 16). However, the parameter *W* does not affect the odd-mode characteristic impedance, which is forced to be short circuited via an electrical wall.

The computed coupling coefficient *K* is shown in Fig. 17 for both normalized slot-coupled width *W* and normalized slot width *S*. For a fixed strip conductor *(G)*, the coupling increases as *S* and *W* increase. It can be noted that the parameter *W* affects considerably the coupling of the proposed coupler.

Since there are various interactions among the parameters involved in the proposed design, a rigorous analysis is necessary for the optimization of the coupler parameters. A commercial computer software package ADS MOMENTUM [7] is used as a CAD tool to design the proposed coupler. First, the top and bottom 50 Ω transmission lines were designed using a duroid substrate (RT/ Duroid 5880) having a dielectric constant of ε_r = 2.2 and thickness h = 0.254 mm. As CPW characteristic impedance is controlled by changing the slot or the strip width, it was necessary to investigate each parameter in order to obtain the right value for the coupling. It was shown that for a fixed substrate thickness and slot width S, the coupling increases as G increases. Second, the length L of the coupler was designed to be a quarter wavelength at 5 GHz. Third, the coupling slot width was determinated in order

to increase the coupling between the CPW lines. Based on this parametric study, the optimum design has the following dimensions: L = 11.9 mm, W = 4.85 mm, S = 1.3 mm, and G = 1.6 mm.
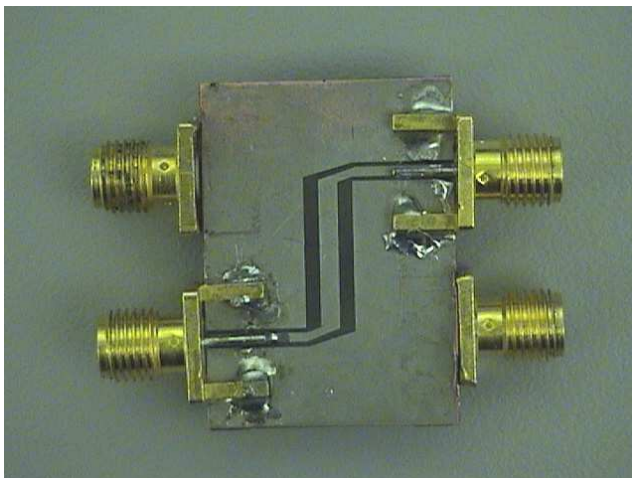

Fig. 18. Photograph of the fabricated circuit prototype

To validate our design, the proposed coupler was fabricated and measured using an HP8772 network analyzer. The photography of the fabricated prototype is shown in Fig. 18. The simulated and measured return loss and the insertion loss are shown in Fig. 19. From these results, it can be concluded that a bandwidth of ~ 4 GHz (~80%) is achieved. The average value of the coupling for the direct port and the coupled port is 3.5 -dB. The return loss and isolation are better than 15 -dB within the operating band. The simulated and measured phase shift between the two ports are plotted in Fig. 20. The phase difference between the direct and coupled ports is approximately 90° across the operating band, which confirms the proposed approach. Furthermore, the comparison between simulated and experimental data shows a good agreement.

(a)
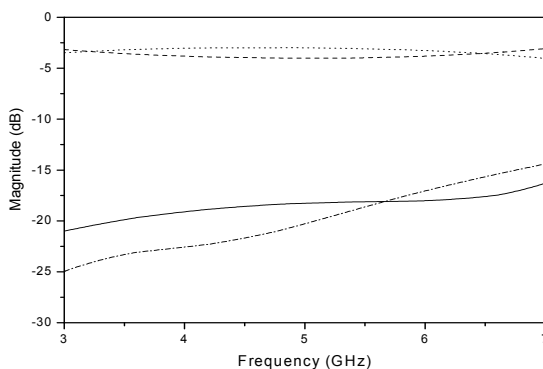
Thank You for previewing this eBook

You can read the full version of this eBook in different formats:

- ➢ HTML (Free /Available to everyone)

- ➢ PDF / TXT (Available to V.I.P. members. Free Standard members can access up to 5 PDF/TXT eBooks per month each month)

- ➢ Epub & Mobipocket (Exclusive to V.I.P. members)

To download this full book, simply select the format you desire below